Journal of Computational Physics 364 (2018) 257–273

Contents lists available at ScienceDirect

Journal of Computational Physics

www.elsevier.com/locate/jcp

Identifying arbitrary parameter zonation using multiple level set functions ☆

Zhiming Lu [a,*], Velimir V. Vesselinov [a], Hongzhuan Lei [b]

[a] Computational Earth Science Group (EES-16), MS T003, Los Alamos National Laboratory, Los Alamos, NM 87545, United States
[b] Department of Scientific Computing, Florida State University, Tallahassee, FL 32306, United States

ARTICLE INFO

Article history:
Received 24 July 2017
Received in revised form 2 February 2018
Accepted 8 March 2018
Available online 14 March 2018

Keywords:
Level set method
Zonation
Parameter identification
Inverse modeling

ABSTRACT

In this paper, we extended the analytical level set method [1,2] for identifying a piecewisely heterogeneous (zonation) binary system to the case with an arbitrary number of materials with unknown material properties. In the developed level set approach, starting from an initial guess, the material interfaces are propagated through iterations such that the residuals between the simulated and observed state variables (hydraulic head) is minimized. We derived an expression for the propagation velocity of the interface between any two materials, which is related to the permeability contrast between the materials on two sides of the interface, the sensitivity of the head to permeability, and the head residual. We also formulated an expression for updating the permeability of all materials, which is consistent with the steepest descent of the objective function. The developed approach has been demonstrated through many examples, ranging from totally synthetic cases to a case where the flow conditions are representative of a groundwater contaminant site at the Los Alamos National Laboratory. These examples indicate that the level set method can successfully identify zonation structures, even if the number of materials in the model domain is not exactly known in advance. Although the evolution of the material zonation depends on the initial guess field, inverse modeling runs starting with different initial guesses fields may converge to the similar final zonation structure. These examples also suggest that identifying interfaces of spatially distributed heterogeneities is more important than estimating their permeability values.

Published by Elsevier Inc.

1. Introduction

Various inverse models have been developed for identifying heterogeneous structures in subsurface environment [3–5]. It is well-known that the inverse problem is typically ill-posed because of limited data available. To avoid the ill-posed problem, one approach is the zonation method [6,7], in which the model domain is divided into a number of zones as a prior, each of which has a uniform parameter value. The zonation method is not only simple but also generally superior to some other methods in case of limited data available [8]. Most of those inverse models focus on identifying the parameter values and determination of the zonation structure is mostly neglected [9]. The main reason is that identifying the zonation structure of an aquifer is much more difficult than estimating the relevant parameter values associated with these zones.

☆ This work was supported by the Los Alamos National Laboratory Environmental Programs.
* Corresponding author.
E-mail address: zhiming@lanl.gov (Z. Lu).

https://doi.org/10.1016/j.jcp.2018.03.016
0021-9991/Published by Elsevier Inc.

Any inaccuracy of a priori assumptions on the number of zones and their shapes and locations about the zonation structure may lead to instability in estimating the piece-wise constant parameter field [9].

Recently, a few approaches have been proposed to identify both the zonation structure and the relevant parameter values. The key difference among these approaches is how to parameterize the zonation structure. There are three commonly-used methods to parameterize the structure: clustering analysis, Voronoi tessellation (VT), and the level set method (LSM).

Ayvaz [10] used a fuzzy c-means clustering method to determine the aquifer parameters and zone structures simultaneously. This method starts with one zone and systematically increases the parameter dimension until the best parameter structure is identified, which was determined from three criteria: residual error, parameter uncertainty and structure discrimination. Eppstein and Dougherty [11] developed an approach that estimates transmissivity values and zonation simultaneously for a steady-state flow problem using an iterative k-mean clustering algorithm. The algorithm works by iteratively applying the standard k-means clustering algorithm, where the centroids of clusters are calculated as the arithmetic mean of the transmissivity of the member zones. The number of clusters is increased each iteration until the predefined cluster tolerance is met within all clusters.

In the VT-base approaches, the optimization process determines an appropriate level of parameter structure complexity, and at each level of complexity the zonation is determined from a set of basis points using the Voronoi tessellation, and the parameters to be optimized include the locations (coordinates) of these basis points and conductivity values at these points [12,13]. In [12], Tsai et al. used sequential global-local optimization to minimize the squared error with a global search for the best parameter values and a local search for basis points. Tsai and Yeh [14] combined the Bayesian estimation and the generalized parameterization method, which is capable of creating a mixture of zonation structure and a continuous distribution of conductivity fields. In [15], Tung and Tan identified the number of zones and their hydraulic conductivity values by combining Voronoi tessellation and simulated annealing. Chiu [16] used Voronoi tessellation to represent the material zonation with different number of basis points, and the coordinates and the conductivity values associated with these points were optimized using differential evolution.

The concept of the level set method (LSM) was first introduced by Osher and Sethian [17] and has been proved to be a very powerful tool for solving problems that involve geometric evolution. This method was initially designed for tracking the motion of a front whose velocity depends on the local curvature. The method has been used in several fields, including shape optimization problems [18], image segmentation [19], and inverse problems [1,20,2,21]. One of the advantages of the level set method is that it is much easier to work with a globally defined function than to keep track of the boundaries of regions of interest, which may split into many regions or merge into larger ones. The level set method requires no *a priori* assumptions on shape, size and locations of zones to be sought or correlation structures of these zones.

In the level set based approaches, the zonation is characterized by one or more level set functions (LSFs). These approaches may be classified into two large groups based on how the LSFs are defined. In the first group, the interface evolves explicitly from solving the Hamilton–Jacobi equation (i.e., level set equation) [1,2,22]. The expression for the propagation velocity of the evolving interface is determined from minimizing the objective function, which is related to the discrepancy between the simulated and observed state variables, such as hydraulic head. In the second group, instead of propagating interfaces directly by specifying interface velocity, they evolve implicitly through updating LSFs using a fixed order of polynomial [23], or some basis functions [24–28], or B-splines [29], or LSFs at some selected grid nodes and LSFs at the rest of grid nodes are calculated from interpolation [20,28].

In this study, we extend the analytical approach in [1,2] for binary fields to parameter zonation identification of any arbitrary number of material zones, through mathematically rigorous derivation. In this approach, the propagation velocity of each interface between any two materials is derived from the minimization of an objective function, which measures the differences between the simulated and observed hydraulic heads. A similar expression for the propagation velocity has been given by Cardiff and Kitanidis [22], but it was not clear how the expression was derived. In addition, as an extension of Lu and Robinson [2], in which the permeability values of two materials are fixed, the permeability values of these material zones are also to be estimated. This method can be used to identify, for example, low-permeability layers in a relatively higher permeability porous media (or vice versa), or highly permeable fault zones in the subsurface.

The rest of paper is organized as follows. Section 2 gives the statement of the inverse problem. Section 3 describes the level set representation of materials zones. In Section 4, we derive analytical expressions for updating (1) material zonation through the propagation velocity of material interfaces and (2) permeability values for all materials. The numerical methods and some implementation issues are discussed in Section 5. Section 6 presents several examples to demonstrate the application of the level set method to identify lower permeable zones in both synthetic and real-world flow problems. Conclusions and discussions are presented in Section 7.

2. Problem statement

We consider transient groundwater flow in confined saturated media satisfying the standard governing equation

$$\nabla \cdot [K_s(\mathbf{x})\nabla h(\mathbf{x},t)] + g(\mathbf{x},t) = S_s \frac{\partial h(\mathbf{x},t)}{\partial t}, \quad \mathbf{x} \in \Omega \tag{1}$$

subject to appropriate initial and boundary conditions [30]. Here $h(\mathbf{x}, t)$ is the hydraulic head, $K_s(\mathbf{x})$ is the saturated hydraulic conductivity, S_s is the specific storage, and Ω is the flow domain. For simplicity, S_s is taken to be constant, because its variability is typically small compared to that of the hydraulic conductivity.

We assume that the saturated hydraulic conductivity field consists of several zones, each of which has a uniform conductivity value. In other words, the conductivity field is a piece-wise constant variable. In the forward modeling, given any conductivity field, one can solve for the hydraulic head from (1), subject to appropriate initial and boundary conditions. In the inverse modeling, however, one tries to estimate the conductivity field using the hydraulic head observed at some selected times and locations.

Now suppose hydraulic heads are observed at n_h locations $\mathbf{x}_1, \mathbf{x}_2, \cdots, \mathbf{x}_{n_h}$, and at n_t times $t_1, t_2, \cdots, t_{n_t}$, arranged in a vector $\mathbf{h}^{(o)} = (h_i^{(o)})$, $i = \overline{1, n_h \times n_t}$. The aim of the inverse analysis is to find the spatial distribution of materials in the domain as well as their conductivity or permeability values. To demonstrate the method, the case of error-free head measurements is examined, though it would be straightforward to include measurement errors in future work.

3. Level set representation of material zonation

For completeness, we briefly introduce the basic idea of the level set method using the case of two materials and then extend the description to the case of multiple materials. Consider an n-dimensional domain Ω for two materials. An $(n-1)$-dimensional subspace $\Gamma \in \Omega$ partitions the domain into a subdomain Ω_1 and this complement $\Omega_2 = \Omega \backslash \Omega_1$, and we define a level set function (LSF) ϕ as

$$\begin{aligned} &\phi(\mathbf{x}) < 0, \quad \text{for } \mathbf{x} \in \Omega_1, \\ &\phi(\mathbf{x}) > 0, \quad \text{for } \mathbf{x} \in \Omega_2, \\ &\phi(\mathbf{x}) = 0, \quad \text{for } \mathbf{x} \in \Gamma. \end{aligned} \tag{2}$$

Note that each subdomain may include a number of disjoint regions. Also note that the LSF and its associated partition are not a one-to-one correspondence. A level set function ϕ uniquely defines a partition, but the same partition can be defined by an infinite number of level set functions. For instance, multiplying ϕ by a non-zero constant will not change the location of the interface and the partition. In numerical implementation, this feature allows us to re-initiate $\phi(\mathbf{x})$ periodically without affecting interface Γ. This is typically done in the iteration process by resetting the value of $\phi(\mathbf{x})$ to the signed distance from $\mathbf{x}$ to the current interface.

The unit outward vector normal to Γ can be written as

$$n(\mathbf{x}) = \frac{\nabla\phi}{|\nabla\phi|}, \tag{3}$$

where $|\nabla\phi|$ is the norm of $\nabla\phi$, $|\nabla\phi|^2 = \nabla\phi \cdot \nabla\phi$. This normal direction at $\mathbf{x} \in \Gamma$ is perpendicular to the tangent plane (or line in two-dimensional cases) to Γ at point $\mathbf{x}$. By this definition, the normal vector $n(\mathbf{x})$ points to the region where $\phi > 0$.

The function ϕ defined in (2) can only partition the domain Ω into disjoint regions with two materials. If there are $M(>2)$ materials in the domain, since it requires $\lfloor \log_2(M) \rfloor + 1$ bits to represent decimal number M in the binary system [31], we need $\lfloor \log_2(M) \rfloor + 1$ LSFs to characterize the partition of M materials; above $\lfloor \cdot \rfloor$ is the floor function mapping a real number r to the largest integer not greater than r. This number could be reduced to $m = \lceil \log_2(M) \rceil$, ($\lceil \cdot \rceil$ is the ceiling function mapping a real number r to the smallest integer not less than r), if we use the binary expression of $(i-1)$ to represent material index i.

Let P be a partition of domain Ω into M materials: $\Omega = \cup_{i=1}^{M} \Omega_i$, where $\Omega_i \cap \Omega_j = \emptyset$ for $i \neq j$, and $\emptyset$ stands for a set of zero measure in the space considered. By definition, any k-dimensional subspace of R^n has measure zero if $k < n$. For instance, for a two-dimensional domain Ω, $\emptyset$ could be a set of points or curves.

The intersection between any two sub-domains Ω_i and Ω_j can be empty or some lower dimension interfaces, such as a curve in the two-dimensional domain or a surface in the three-dimensional domain. Under this partition, the conductivity field can be represented as [20,25,28]

$$K(\mathbf{x}) = \sum_{i=1}^{M} K_i \Psi_i(\phi_1, \cdots, \phi_m), \tag{4}$$

where K_i, $i = \overline{1, M}$ is the conductivity of the ith material, ϕ_j, $j = \overline{1, m}$ are LSFs, and indicator functions Ψ_i are defined as

$$\Psi_i(\phi_1, \cdots, \phi_m) = \prod_{j=1}^{m} R_i(\phi_j), \quad R_i(\phi_j) = \begin{cases} H(\phi_j(\mathbf{x})), & \text{if } b_{ij} = 1 \\ 1 - H(\phi_j(\mathbf{x})), & \text{if } b_{ij} = 0, \end{cases} \tag{5}$$

where $H(x)$ is the Heaviside function with $H(\mathbf{x}) = 1$ for $\mathbf{x} > 0$ and $H(\mathbf{x}) = 0$ for $x \leq 0$. The derivative of the Heaviside function is the Dirac delta function $H'(x) = \delta(x)$. Here b_{ij} is the jth position (from the left to the right, out of the total m positions) in the binary expansion of decimal number $(i-1)_{10} = (b_{i1} b_{i2} \cdots b_{im})_2$, where subscript '2' or '10' represents

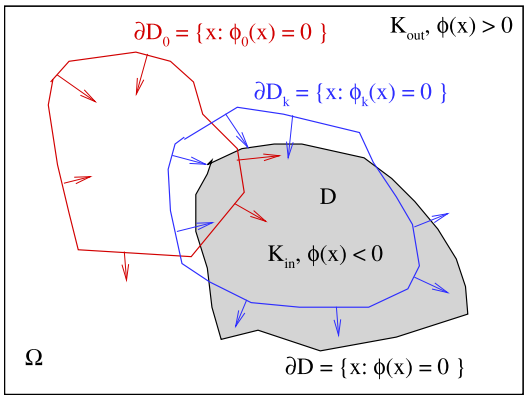

Fig. 1. Schematic diagram illustrating the evolution of the level set function (or equivalently the domain partition defined by the level set function), starting from the initial guess ϕ_0, evolving during the iteration process, and finally approaching to the true partition.

the number in the binary or decimal system. The term b_{ij} has a very clear physical meaning: $b_{ij} = 0$ implying that ϕ_j is negative in material Ω_i or positive otherwise. One obvious advantage of using $(i-1)$ rather than i is that it uses one bit less (or equivalently one less level set function) when M is a power of 2. Note that this definition of R_i^j is slightly different from that in [28], for the purpose of keeping consistency with the zone definition in [2].

The inverse problem described above is to find LSFs $\phi_j(\mathbf{x})$, $j = \overline{1,m}$, such that the hydraulic head field solved using the zone partition $\Omega = \cup_{i=1}^{M}\Omega_i$ characterized by these functions matches the head measurements at various observation locations (e.g., wells) and times. Note that no assumption has been made on the connectedness of Ω_i, i.e., Ω_i could be a disjoint set, or connected but including a number of holes. In addition, there is no assumption made regarding the number of regions, their sizes and locations, correlation structure, or the proportion of these materials. From (4) and (5) it is easy to see that the dependence of the hydraulic head defined in (1) on the material zonation characterized by these level set functions is highly nonlinear, which makes the inverse problem very challenging.

Because the shape, size, and location of set Ω_i are unknown, the level set functions $\phi_j(\mathbf{x})$ are also unknown. In the level set approach, we generate a sequence of partitions $\Omega(\tau) = \cup_{i=1}^{M}\Omega_i(\tau)$ characterized by a sequence of LSFs $\phi_j(\mathbf{x},\tau)$, $j = \overline{1,m}$, such that $\Omega_i(\tau) \to \Omega_i$, where τ represents the index for iteration, as illustrated in Fig. 1 for the case of two materials defined by one LSF. In this iterative process, the number of zones and their shapes, sizes, and locations are sequentially improved. The hydraulic conductivity of these materials can also be updated in this iterative process. The success of this method hinges on finding a strategy for efficiently propagating the boundary of $\Omega_i(\tau)$ such that it approaches to the true unknown Ω_i. This is described in the following sections.

4. Formulation of the inverse problem

The inverse problem described above can be written as a problem of minimizing an objective function:

$$F(K) = \frac{1}{2}\|h(K) - \mathbf{h}_o\|^2, \tag{6}$$

where $\mathbf{h}_o$ is a vector of $n_h \times n_t$ observed heads, K is the hydraulic conductivity or permeability, and h represents an operator that maps the K field to the hydraulic head through solving the flow equation (with appropriate boundary and initial conditions) and then sampling head at measurement locations and times. The vector $h(K)$, denoted as $\mathbf{h}_m$, can be considered as the modeled head at measurement locations and times.

Objective function $F(K)$ is a mapping from the space of function $K(\mathbf{x})$ to a real number. The functional derivative (also known as the Fréchet derivative), $\delta F(K)/\delta K(\mathbf{x})$, quantifies how much the value of $F(K)$ changes if one changes $K(\mathbf{x})$ by a small amount at $\mathbf{x}$. In mathematics, the Fréchet derivative is a derivative defined on Banach spaces. It is usually used to generalize the derivative of a real-valued function of a single real variable to the case of a vector-valued function of multiple real variables [32]. The Fréchet derivative has applications to nonlinear problems throughout mathematical analysis and physical sciences, particularly to the calculus of variations and much of nonlinear analysis and nonlinear functional analysis. The functional derivative can be defined through the following relation [32,33]

$$\delta F(K) = \int_{\Omega} \frac{\delta F(K)}{\delta K(\mathbf{x})}\delta K(\mathbf{x})d\mathbf{x}, \tag{7}$$

which implies that the total change of $F(K)$ upon the variation of the function $K(\mathbf{x})$ is a linear superposition of the local changes summed over the entire domain Ω. The local change can be derived from the derivative of (6) with respect to $K(\mathbf{x})$:

$$\frac{\delta F(K)}{\delta K(\mathbf{x})} = \mathbf{J}^T(K(\mathbf{x}))\,[\mathbf{h}_m - \mathbf{h}_o]\,, \tag{8}$$

where $\mathbf{J}(K(\mathbf{x}))$ is the Jacobian of the head at observation locations/times to conductivity K at location $\mathbf{x}$. Here, $\mathbf{J}$ is a vector of size $n_h \times n_t$, whose components are $J_i = dh_i/dK(\mathbf{x})$, $i = \overline{1, n_h \times n_t}$. In the numerical solution, where the domain is discretized into N grid nodes (or elements), $\mathbf{J}$ is a matrix of $n_h \times n_t$ rows and N columns.

Substituting (8) into (7) yields

$$\delta F(K) = \int_\Omega \mathbf{J}^T(K)\,[\mathbf{h}_m - \mathbf{h}_o]\,\delta K(\mathbf{x}) d\mathbf{x}, \tag{9}$$

where the integrand is a scalar. The variation δK can be derived from (4). Such variations might be due to the variation of conductivity of each material and/or the variation of interfaces among these materials. As the result, (9) can be written as two integrals, one accounting for the variation of the material interfaces and the other for the variation of conductivity values. Both of these two factors can be considered in the inverse model, for instance, by alternatively updating conductivity values and interface locations. For simplicity in derivation and discussion, we consider these two factors separately.

4.1. Variation of material interfaces

For a special case of two materials with unknown interfaces, following [1], Lu and Robinson [2] reduce the integral over the domain Ω in (9) to an integral over the interface of material zones by graphically relating δK to the propagation of interfaces. For a general case with an arbitrary number of materials, it is not obvious to extend the above approach. Without mathematical derivations, Cardiff and Kitanidis [22] gave an expression of δF as an integral over all interfaces defined by $\{\mathbf{x} : \phi_i(\mathbf{x}) = 0; i = \overline{1, m}\}$, while the integrand is proportional to the contrast of the conductivity field on the two sides of the interface. Here we propose a theoretically rigorous way to deal with the general case of an arbitrary number of material zones.

Taking the variation of (4) and noting $dH(x)/dx = \delta(x)$ gives

$$\delta K(\mathbf{x}) = \sum_{j=1}^{m} \delta(\phi_j)\delta\phi_j \sum_{i=1}^{M} (-1)^{b_{ij}+1} K_i \prod_{\substack{k=1 \\ k\neq j}}^{m} R_i(\phi_k(\mathbf{x})), \tag{10}$$

where $\delta(\phi_j)$ is the Dirac delta function with $\delta(\phi_j) = 1$ for $\phi_j > 0$ and $\delta(\phi_j) = 0$ otherwise, while $\delta\phi_j$ stands for the variation of ϕ_j. Substituting (10) into (9) and utilizing a property of the delta function:

$$\int_\Omega f(\mathbf{x})\delta(\phi(\mathbf{x}))d\mathbf{x} = \int_{\{\mathbf{x}:\phi(\mathbf{x})=0\}} \frac{f(\mathbf{x})}{|\nabla\phi|} d\mathbf{x}, \tag{11}$$

where $f(\mathbf{x})$ is any function, we have

$$\delta F(K) = \sum_{j=1}^{m} \int_{\{\mathbf{x}:\phi_j(\mathbf{x})=0\}} \beta(K) \frac{\delta\phi_j}{|\nabla\phi_j|} \sum_{i=1}^{M} (-1)^{b_{ij}+1} K_i \prod_{\substack{k=1 \\ k\neq j}}^{m} R_i(\phi_k(\mathbf{x})) d\mathbf{x}, \tag{12}$$

where $\beta(K) = \mathbf{J}^T(K)\,[\mathbf{h}_m - \mathbf{h}_o]$ is a scalar. Similar to the case of two materials, the integration now is over all surfaces defined by $\{\mathbf{x} : \phi_j(\mathbf{x}) = 0\}$, $j = \overline{1, m}$. As seen later, these surfaces may overlap each other. From (4) and (5), we also note that each of these surfaces may include a number of interfaces that separate different materials and can be written as, for any $j = \overline{1, m}$,

$$\{\mathbf{x} : \phi_j(\mathbf{x}) = 0\} = \left(\bigcup_{p:\, b_{pj}=0} \Omega_p \right) \bigcap \left(\bigcup_{q:\, b_{qj}=1} \Omega_q \right) = \bigcup_{b_{pj}=0, b_{qj}=1} \Omega_{pq}^{(j)}, \tag{13}$$

where $\Omega_{pq}^{(j)}$ denotes the interface between Ω_p and Ω_q characterized by the jth LSF with $\phi_j(\mathbf{x}) < 0$ for $\mathbf{x} \in \Omega_p$ and $\phi_j(\mathbf{x}) > 0$ for $\mathbf{x} \in \Omega_q$. Any physical interface between Ω_p and Ω_q, denoted as $\Omega_{pq} = \Omega_p \cap \Omega_q$, if it exists, may include one or more $\Omega_{pq}^{(j)}$. Fig. 2 illustrates an example for $M = 4$ materials characterized by $m = 2$ level set functions. This example includes all possible interfaces for the case of 4 materials. As seen from the figure, while most of interfaces such as Ω_{12} and Ω_{13} are uniquely defined by one LSF, some of interfaces, such as Ω_{14} and Ω_{23}, are defined by more than one LSF. In the latter case, one needs to distinguish the LSF associated with the interfaces, such as $\Omega_{14}^{(1)}$ and $\Omega_{14}^{(2)}$. In the former case, for the sake of clarity, we also specify the LSF by which the interface is defined (i.e., $\Omega_{12}^{(2)}$ or $\Omega_{13}^{(1)}$). As a result, surfaces $\{\mathbf{x} : \phi_j(\mathbf{x}) = 0\}$ could

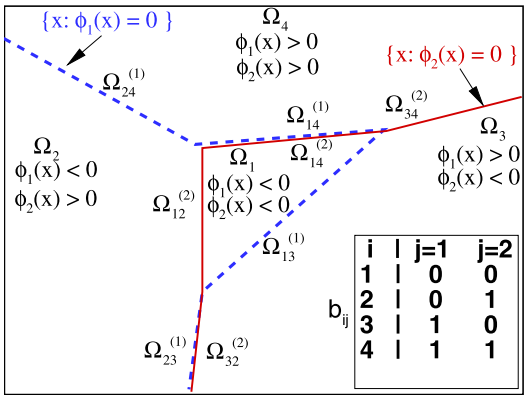

Fig. 2. Schematic representation of possible interface locations for the case of 4 materials characterized by two LSFs. Note that some of the material interfaces are defined by more than one LSF (such as Ω_{14} and Ω_{23}). The table in the right lower corner shows the matrix $B = (b_{ij})_{4\times 2}$ for the case with up to four materials. (For interpretation of the colors in the figure(s), the reader is referred to the web version of this article.)

be overlapping each other for different j. For instance, from Fig. 2 it is seen (dashed blue segments for ϕ_1 and solid red segments for ϕ_2):

$$\begin{aligned}\{\mathbf{x}:\phi_1(\mathbf{x})=0\} &= \Omega_{13}^{(1)}\cup\Omega_{23}^{(1)}\cup\Omega_{14}^{(1)}\cup\Omega_{24}^{(1)},\\ \{\mathbf{x}:\phi_2(\mathbf{x})=0\} &= \Omega_{12}^{(2)}\cup\Omega_{32}^{(2)}\cup\Omega_{14}^{(2)}\cup\Omega_{34}^{(2)}.\end{aligned} \tag{14}$$

Here $\{\mathbf{x}:\phi_1(\mathbf{x})=0\}$ and $\{\mathbf{x}:\phi_2(\mathbf{x})=0\}$ share the same interfaces Ω_{14} and Ω_{23}. Equations (13) and (14) indicate that the summation in (12) may be written equivalently as a summation over all interfaces:

$$\delta F(K) = \sum_{\substack{p,q=1\\ p\neq q}}^{M}\int_{\Omega_{pq}}\sum_{\substack{j:b_{pj}=0\\ \&b_{qj}=1}}^{m}\beta(K)\frac{\delta\phi_j}{|\nabla\phi_j|}\sum_{i=1}^{M}(-1)^{b_{ij}+1}K_i\prod_{\substack{k=1\\ k\neq j}}^{m}R_i(\phi_k(\mathbf{x}))d\mathbf{x}. \tag{15}$$

To further simplify (15), we need to determine $\delta\phi_j/|\nabla\phi_j|$ on each interface $\Omega_{pq}^{(j)}$. Taking the variation of equation $\phi_j(\mathbf{x})=0$ on interface $\Omega_{pq}^{(j)}$ gives

$$\delta\phi_j(\mathbf{x}) + \nabla\phi_j(\mathbf{x})\cdot\delta\mathbf{x} = 0, \quad \mathbf{x}\in\Omega_{pq}^{(j)}. \tag{16}$$

We restrict the displacement, $\delta\mathbf{x}$, along the normal direction on the interface Ω_{pq}

$$\delta\mathbf{x} = \alpha_{pq}(\mathbf{x})\mathbf{n}_{pq}^{(j)}(\mathbf{x}), \tag{17}$$

where $\mathbf{n}_{pq}^{(j)}(\mathbf{x})$ is the unit outward normal vector, defined as $\mathbf{n}_{pq}^{(j)}(\mathbf{x}) = \nabla\phi_j(\mathbf{x})/|\nabla\phi_j|$, as seen in (3). Here $\alpha_{pq}(\mathbf{x})$ can be considered as the propagation velocity of the physical interface Ω_{pq}, which should be independent of j. For example, notationally we have $\Omega_{14}^{(1)}$ and $\Omega_{14}^{(2)}$ for the case of 4 materials described above, but they represent the same physical interface and should propagate at the same velocity. Combining (16) and (17) yields

$$\frac{\delta\phi_j(\mathbf{x})}{|\nabla\phi_j(\mathbf{x})|} = -\alpha_{pq}(\mathbf{x}), \quad \mathbf{x}\in\Omega_{pq}. \tag{18}$$

Substituting this expression into (15) yields

$$\delta F(K) = -\sum_{\substack{p,q=1\\ p\neq q}}^{M}\int_{\Omega_{pq}}\alpha_{pq}(\mathbf{x})\beta(K)\sum_{\substack{j:b_{pj}=0\\ \&b_{qj}=1}}^{m}\sum_{i=1}^{M}(-1)^{b_{ij}+1}K_i\prod_{\substack{k=1\\ k\neq j}}^{m}R_i(\phi_k(\mathbf{x}))d\mathbf{x}, \tag{19}$$

where the first summation is over all possible interfaces, while the second summation includes all level set functions characterizing each individual interface (such as $\Omega_{14}^{(1)}$ and $\Omega_{14}^{(2)}$ in the previous example). For any interface that was defined by a single level set function, the second summation reduces to a single term.

To ensure that $F(K)$ is always decreasing in the iteration process, we choose α_{pq} as:

$$\alpha_{pq}(\mathbf{x}) = \beta(K)\sum_{\substack{j:b_{pj}=0\\ \&b_{qj}=1}}^{m}\sum_{i=1}^{M}(-1)^{b_{ij}+1}K_i\prod_{\substack{k=1\\ k\neq j}}^{m}R_i(\phi_k(\mathbf{x})), \tag{20}$$

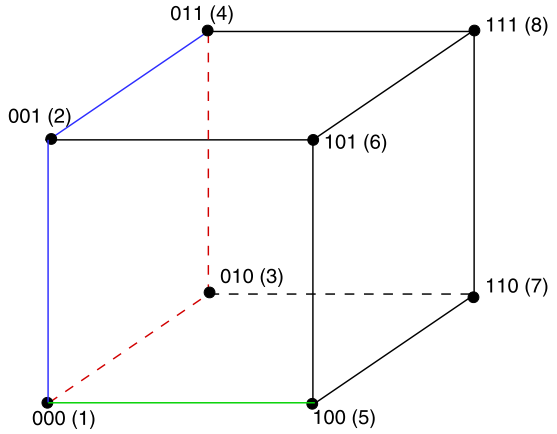

Fig. 3. 3-bit binary cube for finding the Hamming distances. The numbers in parentheses are material indexes, and 3-digit numbers can be viewed either as the row vectors in binary matrix B (see Table 1) or strings in the Hamming space.

and (19) reduces to

$$\delta F(p) = -\sum_{p,q} \int_{\Omega_{pq}} [\alpha_{pq}(\mathbf{x})]^2 d\mathbf{x}, \tag{21}$$

which is always non-positive. We can also choose α_{pq} to be the right side of (20) scaled by any positive number. This will also keep $F(K)$ decreasing. It is noted that the propagation rate $\alpha_{pq}(\mathbf{x})$ depends on the location $\mathbf{x}$ on Ω_{pq}, in part through $\mathbf{J}(K)$, which is the sensitivity of head at all measurement locations/times to conductivity on $\mathbf{x} \in \Omega_{pq}$.

The expression for α_{pq} in (20) can be simplified further by introducing the concept of the Hamming space and Hamming distance. Let $\mathcal{H} = \{0, 1\}$, and the m-dimensional Hamming Space $\mathcal{H}^m$ consists of 2^m strings of length m. Each point $x \in \mathcal{H}^m$ is a string $x = (x_1 x_2 \cdots x_m)$ of zeros and ones. For any two points $x, y \in \mathcal{H}^m$, their Hamming distance $d_{\mathcal{H}}(x, y)$ is the number of positions at which the corresponding strings differ, i.e., $d_{\mathcal{H}}(x, y) = |\{i : x_i \neq y_i\}|$, where $|\cdot|$ stands for the cardinality (size) of the set. This distance represents the minimum number of substitutions required to change one string to the other. For an m-dimensional Hamming space, the number of string pairs that have a distance d will be $N_m^d = 2^{m-1} C_m^d$, where C_m^d, also written as $\binom{m}{d}$, is the combination of choosing d objects from m objects without repetition, and the number of all possible physical interfaces is $\sum_{d=1}^{m} 2^{m-1} C_m^d = 2^{m-1}(2^m - 1)$. An example of the Hamming space for $m = 3$ is shown in Fig. 3. In this diagram, there are $2^m = 8$ vertexes and each vertex represents one material (labeled in parentheses). The Hamming distance between any pair of vertexes is the number of edges in a shortest path connecting the pair. For instance, $d_H(000, 100) = 1$ (green path) and $d_H(000, 011) = 2$ (blue path or red path). The numbers of pairs with distance 1, 2, and 3, for this case are $N_3^1 = 12$, $N_3^2 = 12$, and $N_3^3 = 4$, respectively, and there are $2^2(2^3 - 1) = 28$ possible physical interfaces. This diagram shows not only the possible interfaces between different materials, but also the LSFs that characterize these interfaces. For example, the interface between materials 1 (string 000) and 5 (string 100), Ω_{15}, is described by the level set function ϕ_1 because two strings differ at position 1, and the interface between materials 1 (string 000) and 4 (string 011) is characterized by both ϕ_2 and ϕ_3 because two strings differ at positions 2 and 3.

Now we are ready to simplify α_{pq} in (20). We first consider a simple case of Ω_{pq} in which the Hamming distance between $(p-1)_{10} = (b_{p1} b_{p2} \cdots b_{pm})_2$ and $(q-1)_{10} = (b_{q1} b_{q2} \cdots b_{qm})_2$ is one. Assume without loss of generality that these two binary numbers differ at the nth position, i.e., $b_{pn} = 0$, $b_{qn} = 1$, and $b_{pj} = b_{qj}$ for $j \neq n$. From (20), the expression for α_{pq} may be written as

$$\alpha_{pq}(\mathbf{x}) = \alpha_{pq}^{(n)}(\mathbf{x}) = \beta(K) \sum_{i=1}^{M} (-1)^{b_{in}+1} K_i \prod_{\substack{k=1 \\ k \neq n}}^{m} R_i(\phi_k(\mathbf{x})). \tag{22}$$

Now, let's start with first column of the binary matrix $B = (b_{ij})_{M \times m}$ (refer to Table 1) that satisfies $b_{pk} = b_{qk}$. If $b_{pk} = b_{qk} = 0$, the level set function $\phi_k < 0$ on Ω_{pq}, and $H(\phi_k) = 0$. By the definition of $R_i(\phi_k)$, any material i that has a '1' on the kth position (i.e., $b_{ik} = 1$) in the binary representation of $(i-1)$ will disappear from the above summation. On the other hand, if $b_{pk} = b_{qk} = 1$, the level set function $\phi_k > 0$ on Ω_{pq}, and $H(\phi_k) = 1$, and any material i that has a '0' on the kth position (i.e., $b_{ik} = 0$) in the binary representation of $(i-1)$ will disappear from the above summation. In other words, if $b_{pk} = b_{qk}$, then any material i with $b_{ik} \neq b_{pk}$ will vanish from the summation in (22). This process will cross-out 2^{m-1} terms from (22). Repeat this process $m-1$ times for all $m-1$ columns that satisfy $b_{pj} = b_{qj}$ (recalling that $b_{pn} \neq b_{qn}$). Since each column in the binary matrix B of 2^m rows contains 2^{m-1} ones and 2^{m-1} zeros, the first cross-out will delete 2^{m-1} terms, and the second time will delete only half of this amount (i.e., 2^{m-2}), because the other half have been deleted in the first round, and

Table 1
Binary representation of material zonation up to eight materials.

Material i	Binary $i-1$	$R_i(\phi_1)$	$R_i(\phi_2)$	$R_i(\phi_3)$
1	0 0 0	$1-H(\phi_1)$	$1-H(\phi_2)$	$1-H(\phi_3)$
2	0 0 1	$1-H(\phi_1)$	$1-H(\phi_2)$	$H(\phi_3)$
3	0 1 0	$1-H(\phi_1)$	$H(\phi_2)$	$1-H(\phi_3)$
4	0 1 1	$1-H(\phi_1)$	$H(\phi_2)$	$H(\phi_3)$
5	1 0 0	$H(\phi_1)$	$1-H(\phi_2)$	$1-H(\phi_3)$
6	1 0 1	$H(\phi_1)$	$1-H(\phi_2)$	$H(\phi_3)$
7	1 1 0	$H(\phi_1)$	$H(\phi_2)$	$1-H(\phi_3)$
8	1 1 1	$H(\phi_1)$	$H(\phi_2)$	$H(\phi_3)$

so on. Therefore, the total number of materials crossed out from this procedure will be $2^{m-1}+2^{m-2}+\cdots+2$, which equals 2^m-2. In other words, the right side of (22) reduces to $\alpha_{pq}(\mathbf{x})=\beta(K)\left(K_q-K_p\right)$ when the Hamming distance between vertexes p and q (or equivalently the binary strings of $p-1$ and $q-1$) is one.

If the Hamming distance between the binary expressions of $p-1$ and $q-1$, denoted as d, is greater than one, we may decompose the path from vertex p to vertex q into d steps, each of which involves two vertexes that has a Hamming distance of one. In this case, we may write $\alpha_{pq}=\alpha_{pi_1}^{(j_1)}+\alpha_{i_1i_2}^{(j_2)}+\cdots+\alpha_{i_{d-1}q}^{(j_d)}$, where each pair of indexes in the subscript have a Hamming distance of one, and their binary representations differ at one position specified in the superscript. From the previous discussion on the case of Hamming distance of one, it is easy to see $\alpha_{pq}(\mathbf{x})=\beta(K)\left(K_{i_1}-K_p\right)+\beta(K)\left(K_{i_2}-K_{i_1}\right)+\cdots+\beta(K)\left(K_q-K_{i_{d-1}}\right)=\beta(K)(K_q-K_p)$. For instance, on interface Ω_{14}, using the blue path in Fig. 3, the propagation velocity $\alpha_{14}(\mathbf{x})=\alpha_{14}^{(2)}+\alpha_{14}^{(3)}$ can be re-written as

$$\begin{aligned}\alpha_{14}(\mathbf{x}) &= \alpha_{12}^{(3)}(\mathbf{x})+\alpha_{24}^{(2)}(\mathbf{x})\\ &= \beta(K)\left(K_2-K_1\right)+\beta(K)\left(K_4-K_2\right)=\beta(K)\left(K_4-K_1\right).\end{aligned} \tag{23}$$

The same result can be obtained by using the red path in the figure, $\alpha_{14}=\alpha_{13}^{(2)}+\alpha_{34}^{(3)}=\beta(K)\left(K_4-K_1\right)$. Finally, we can write the propagation of any interface Ω_{pq} as

$$\alpha_{pq}(\mathbf{x})=\beta(K)\left(K_q-K_p\right). \tag{24}$$

This expression suggests that the propagation velocity at any point $\mathbf{x}$ on an interface is proportional to the permeability contrast between the materials on both sides of the interface. In particular, for a binary conductivity field, the corresponding propagation velocity is

$$\alpha_{12}(\mathbf{x})=\beta(K)\left(K_2-K_1\right), \tag{25}$$

which is the same as the one given in Lu and Robinson [2], except for a proportional constant.

The final step is to derive equations for the evolution of ϕ_j, $j=\overline{1,m}$. Substituting the variation of $\mathbf{x}$ in (17) into (16) and recalling the definition of $\mathbf{n}_{pq}^{(j)}=\nabla\phi_j/|\nabla\phi_j|$, we have

$$\delta\phi_j(\mathbf{x})+\alpha_j(\mathbf{x})|\nabla\phi_j(\mathbf{x})|=0, \tag{26}$$

where $\alpha_j(\mathbf{x})$ is the assembled $\alpha_{pq}(\mathbf{x})$ for $\phi_j(\mathbf{x})$, as α_{pq} is only defined on interface Ω_{pq}. The propagation velocity $\alpha_j(\mathbf{x})$ varies for different LSFs because they involve different interfaces Ω_{pq}. If the function $\phi_j(\mathbf{x})$ is expressed as a function of both $\mathbf{x}$ and an artificial time τ, $\phi_j=\phi_j(\mathbf{x},\tau)$, the evolution of $\phi_j(\mathbf{x},\tau)$ accordingly defines the evolution of the partition $\Omega=\cup_{i=1}^{M}\Omega_i(\tau)$ over time τ:

$$\frac{\partial\phi_j(\mathbf{x},\tau)}{\partial\tau}+\alpha_j(\mathbf{x},\tau)|\nabla\phi_j(\mathbf{x},\tau)|=0, \tag{27}$$

with an initial condition $\phi_j(\mathbf{x},0)=\phi_j^0(\mathbf{x})$. This equation is called Hamilton–Jacobi equation (or the level set equation). For sufficiently large τ, $\{\mathbf{x}:\phi_j(\mathbf{x},\tau)=0\}$, $j=\overline{1,m}$, define the spatial distribution of M materials, which is the final solution to the inverse problem.

4.2. Variation of conductivity values

The variation δK due to the variation of each individual conductivity K_i alone can be derived from (4) as

$$\delta K(\mathbf{x})=\sum_{i=1}^{M}\Psi_i(\phi_1,\cdots,\phi_m)\delta K_i. \tag{28}$$

Substituting this into (9) and using the property of Ψ_i yields:

$$\delta F(K) = \sum_{i=1}^{M} \int_{\Omega_i} \mathbf{J}^T(K)\,[\mathbf{h}_m - \mathbf{h}_o]\,\delta K_i d\mathbf{x}. \tag{29}$$

This expression is valid for both piece-wise conductivity fields and continuous conductivity fields that vary within each individual material. If we consider the piece-wise conductivity field only, i.e., K_i is a constant in Ω_i, the above equation reduces to

$$\delta F(K) = \sum_{i=1}^{M} \delta K_i \int_{\Omega_i} \mathbf{J}^T(K)\,[\mathbf{h}_m - \mathbf{h}_o]\,d\mathbf{x}. \tag{30}$$

In the iterative inverse process, if we update the current K_i by δK_i determined from the following expression:

$$\delta K_i = -\int_{\Omega_i} \mathbf{J}^T(K)\,[\mathbf{h}_m - \mathbf{h}_o]\,d\mathbf{x}, \tag{31}$$

the variation of the objective function becomes

$$\delta F(K) = -\sum_{i=1}^{M} (\delta K_i)^2, \tag{32}$$

which is always non-positive. It should be noted that, although permeability in each subdomain Ω_i is uniform, the sensitivity $\mathbf{J}^T(K)$ is not uniform in each subdomain, because this sensitivity depends not only the permeability field but also the flow conditions (initial and boundary conditions, as well as sources/sinks).

Equation (31) represents the integral of all residuals between the simulated and observed heads, weighted by the head sensitivity at observation locations and times to the conductivity in Ω_i. Suppose that dh_l/dK_i, the sensitivity of head at observation location k and time j, where $l = (k-1)*n_t + j$, is positive. If at one moment (iteration) the modeled head $h_l^{(m)}$ is greater than the observed head $h_l^{(o)}$, then the contribution $-dh_l/dK_i\,(h_l^{(m)} - h_l^{(o)})$ to δK_i will be negative, which tends to reduce K_i and thus $h_l^{(m)}$ in the next iteration. On the other hand, if $h_l^{(m)} < h_l^{(o)}$, the effect of this observation to δK_i will be positive, which then tends to increase K_i in the next iteration and thus increases $h_l^{(m)}$.

5. Numerical implementation

In this section, we discuss the numerical implementation and some technical issues in the implementation.

5.1. Sensitivity calculation

A prerequisite for this gradient-based level set method is the sensitivity of state variables (e.g., steady-state or transient hydraulic head) to the permeability field. One efficient way to calculate the sensitivity is the adjoint method [34–36]. In general, for each observation location, this involves solving the adjoint equation and then integrating the production of the gradient of the solution (called the adjoint variable) and that of the mean head field, over the model domain for a correlated permeability field or over the mesh element that contains observation location for the case of an uncorrelated field [36]. Details can be found in Lu and Vesselinov [36]. The adjoint equation has the same format as the original flow equation but is subject to homogeneous boundary conditions and a terminal condition instead of the initial condition in the original flow equation. The effect of sources/sinks and boundary conditions on the sensitivity is taken into account through the gradient of the mean head field in the integrand. Typically the adjoint equation has to be solved numerically and integration is also calculated numerically. However, analytical expressions for the head sensitivity to permeability can be derived for regular flow domains and boundary conditions as in this study [36].

5.2. Solving for level set functions

The second important component of this level set method is solving the Hamilton–Jacobi equation or the level set equation, (27), which is an initial value problem for each LSF. All LSFs are defined in the entire model domain and their values at any point in the domain are initialized using the initial guess material distribution by assigning its signed distance to some material interfaces, as described below. Unlike the binary system in which the material distribution is characterized by a single LSF and the function value has different signs on both sides of material interfaces (see Equ. (2)), for a porous medium with more than two materials, an LSF does not always change the sign across an interface. For instance, in Fig. 2, $\phi_1(x)$ is negative in both Ω_1 and Ω_2, and so it does not change the sign across the interface between these two materials.

We utilize matrix $B = (b_{ij})_{M\times m}$ and the initial guess field to initialize all LSFs. For each LSF ϕ_j and each node n in the numerical grid, if the material type at this node is k, we will check b_{kj}. If $b_{kj} = 0$, we need to find the minimum distance between node n and all nodes satisfying $b_{*j} = 1$, where wildcard $*$ stands for any number. Otherwise (i.e., $b_{kj} = 1$), we need to find the minimum distance between this node n and all nodes satisfying $b_{*j} = 0$. In the former case, we assign the negative value of the minimum distance to $\phi_j(n)$, and in the latter case, we assign the minimum distance to $\phi_j(n)$. Let's take a case with four material as an example (Fig. 2). The matrix B for this case is listed in the right lower corner of the figure. For LSF ϕ_1 (column labeled 'j = 1'), if the material type at a node n is 1 or 2 ($b_{11} = 0$ and $b_{21} = 0$), we find the minimum distance from this node to all nodes with material type 3 or 4. The logic is that the set $\{\mathbf{x} : \phi_1(\mathbf{x}) = 0\}$ separates $\Omega_1 \cup \Omega_2$ and $\Omega_3 \cup \Omega_4$, and the sign of ϕ_1 at node n is determined by b_{kj} being 0 or 1. The initial LSF ϕ_2 can be derived similarly.

Once all LSFs are initialized, iteratively updating these functions is straightforward. The steady-state or transient flow equation is solved using the current permeability field (or initial guess field for the first iteration), and the residual between the simulated and observed heads at measurement times and locations is calculated. The iterative process stops if the residual is smaller than a prescribed stopping criterion or the maximum number of iterations has reached. Otherwise, the head differences, together with the head sensitivity, are used to calculate the propagation velocity $\alpha_{pq}(\mathbf{x})$ on interface Ω_{pq} (if it exists), using (24). From (27), the LSF ϕ_j can be updated explicitly through

$$\phi_j(\mathbf{x}, \tau + \Delta\tau) = \phi_j(\mathbf{x}, \tau) - \alpha_j(\mathbf{x}, \tau)|\nabla\phi_j(\mathbf{x}, \tau)|\Delta\tau, \tag{33}$$

where $\nabla\phi_j(\mathbf{x}, \tau)$ is the gradient of the current ϕ_j, and $\Delta\tau$ is determined from the propagation velocity in such a way that the maximum displacement at any location of all interfaces is less than the minimum size of elements in the grid. These new LSFs are then applied to update the new permeability zonation $K(\mathbf{x})$ through (4) and (5), which is used in the next iteration.

In updating LSFs using (33), they may become irregular after some period of time [37]. One way to alleviate this problem is by periodically re-initializing the LSFs to the signed distance function using the current material zonation, as described above. The rationale behind this re-initialization process is that any zonation determined from the LSFs depends on the signs of LSFs rather than their absolute values, and therefore such a re-initialization will not change the zonation but makes the LSFs well behaved.

5.3. Updating permeability values

The permeability value for each material is updated using (31). Recalling that $\mathbf{J}^T(K_i)[\mathbf{h}_m - \mathbf{h}_o]$ is in fact the gradient of the objective function $F(K)$, (31) implies that the update to each conductivity K_i will be in the down-gradient direction, and the vector δK will be in the steepest descent of objective function $F(K)$. In practice, we may fix the permeability value for the background material while leave the permeability values for those embedded (unobserved) materials to be estimated. Our experience is that we may simply update the material zonation first and use some guess permeability values in early iterations, and start to update permeability values when the material zonation is more-or-less stabilized. This is because the variable permeability values for embedded materials do not significantly affect the reduction of the objective function.

6. Illustrative examples

In this section, we will demonstrate zonation identification using the level set method through many examples, ranging from totally synthetic cases to a case where the flow conditions are taken from a real site.

6.1. Updating both zonation structure and permeability

In the first example (Case 1), two lower permeable zones (log permeability values of $\log K_1 = -12$ and $\log K_2 = -14$) are embedded in the background porous medium with a log permeability value of $\log K_3 = -9$. The simulation domain and the locations of the embedded zones are the same as the example in [2], except that the two embedded lower permeability zones have different permeability values instead of the same value.

The two-dimensional square domain of size 100 m × 100 m is uniformly discretized into elements of 1 m × 1 m. The boundary conditions are given as: prescribed constant heads at the left (10.5 m) and right (10.0 m) boundaries, and no-flow on two lateral boundaries. The steady-state flow equation subject to the above boundary conditions is solved with the true permeability field (Fig. 4a), using the finite-element heat- and mass-transfer code (FEHM) [38], which is developed at Los Alamos National Laboratory. The code uses the control volume finite element method, and is capable of simulating coupled multiple phase flow and solute transport in geologically complex subsurface environment. The simulated hydraulic head at 36 locations, indicated as green dots in the figure, are taken as the measurements.

The goal is then to identify the spatial distribution of three materials and their permeability values using the head measurements. Since we do not have sufficient information about the shapes of these embedded lower permeable zones, we simply start with two discs to represent the initial shapes of these zones (Fig. 4b). It is assumed that the permeability of the background material is known and fixed at $\log K_3 = -9$, while the spatial distribution of the lower permeability materials

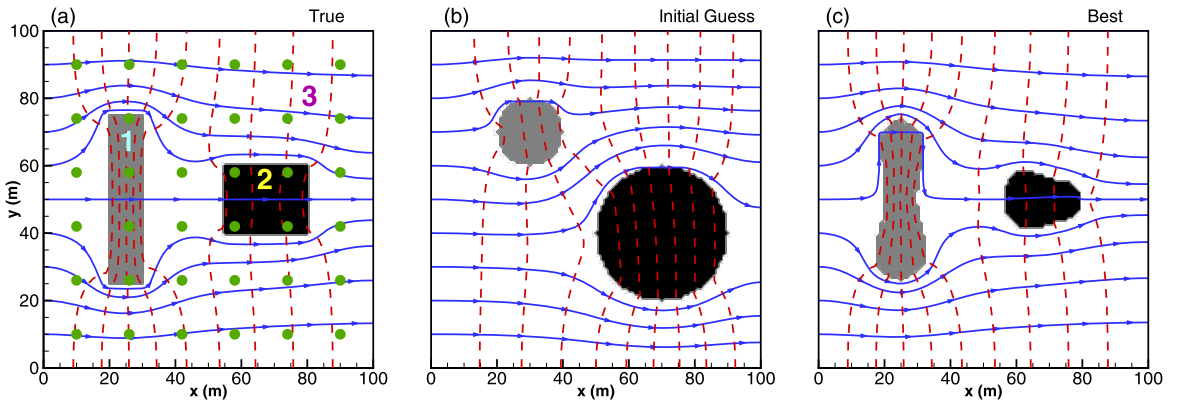

Fig. 4. Comparison of (a) the true permeability field, (b) initial guess, and (c) the best results in terms of the minimum residual from 700 iterations, for Case 1, which has three materials.

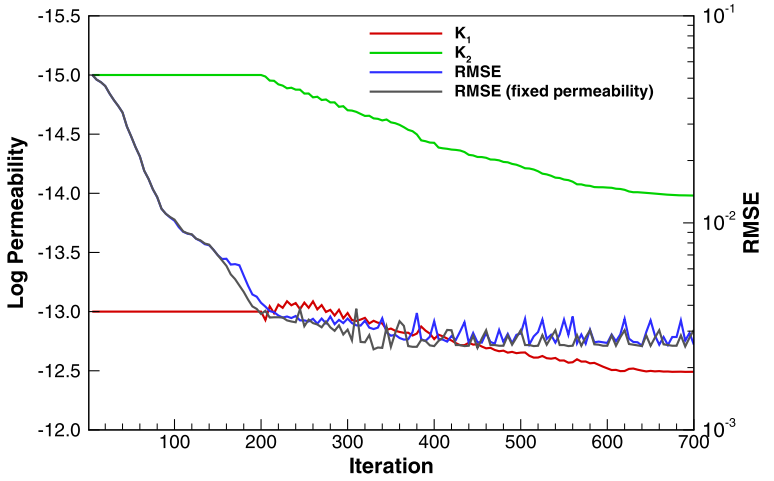

Fig. 5. The permeability values for three materials and the root mean squared error (RMSE) as functions of the iteration number, Case 1.

and their permeability are unknown. The initial log permeability values of these lower-permeability materials are assigned as $\log K_1 = -13$ and $\log K_2 = -15$, which deviate from their true values by one order of magnitude. We solve steady-state flow equation with the initial guess permeability field, then update the material zonation by calculating the propagation velocity of any interface Ω_{pq} using (24), updating the level set functions ϕ_i, indicator functions Ψ_i, and the permeability zonation $K(\mathbf{x})$ using (27), (5), and (4), respectively. In the first 200 iterations, we only update the spatial distribution of the materials, and the permeability values are fixed at the initial guess values. After 200 iterations, the permeability values of materials are updated every 5 iterations using (31). This process continues until the maximum number of iterations is reached or the root mean squared error (RMSE) is smaller than the prescribed value. The true permeability field, the initial guess, and the best inversion results are compared in Fig. 4, where the best inversion field is selected based on the smallest RMSE out of all 700 iterations. It is seen from the figure that the inversion results are quite similar to the true field, except that the lower permeable zones from the inversion results have smooth corners rather than the sharp corners as in the true field. The reason is that the head measurements are not sensitive to the shape of the corners, unless measurement locations are very close to these corners. As seen later in Section 6.3, the estimated material zonation will be greatly improved by adding more measurements.

This gradient-based approach ensures that the RMSE will be reduced over the iteration process. Fig. 5 shows the RMSE (blue curve) as a function of the iteration number up to 700 iterations. In general, the RMSE reduces with iterations, great reduction of the RMSE is observed at early iterations, and the RMSE is stabilized after about 200 iterations. Fig. 5 also depicts the evolution of log permeability of lower permeability materials over iterations, which is allowed to be adjusted after 200 iterations. The figure indicates that the permeabilities of the lower permeable materials varies over iteration and become close to the true values.

For the purpose of comparison, we also ran a similar inverse model where the only difference from the previous model is that the permeability for all materials are fixed at the true values. The reduction of RMSE for this run is also depicted in Fig. 5 (the black curve). Several important remarks can be made from this comparison. First, the RMSEs from two inverse

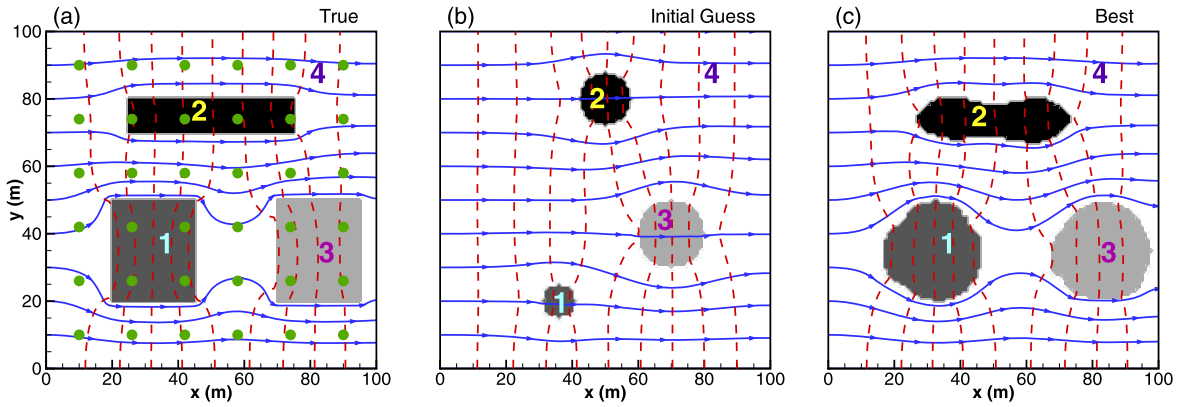

Fig. 6. Comparison of (a) the true permeability field, (b) initial guess, and (c) the best inversion results in terms of the smallest RMSE in 700 iterations, for Case 2.

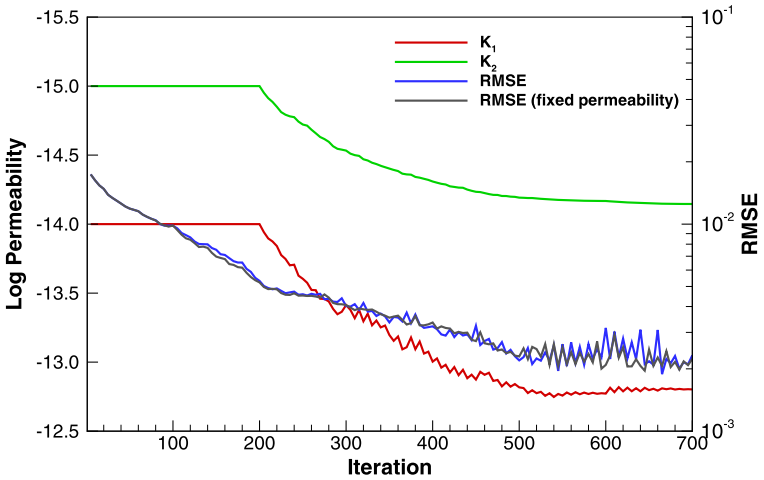

Fig. 7. The permeability values and the root mean squared error (RMSE) as functions of the iteration number, Case 2.

models are very close. In particular, at the early iterations, the RMSEs are overlapping, which means that the RMSE is not sensitive to the initial guess of the lower permeable zones. Second, at about 150 iterations, the RMSE from the run with true permeability values is smaller than that from the run with guess permeability values, which indicates that the effect of permeability values appears when the spatial distribution of the materials are close to the true one. Furthermore, it is important to note that, the permeabilities of two lower permeable materials have been adjusted significantly but the change of the RMSE is very small, which may suggest that in inverse modeling, it is more important to identify the shapes and locations of heterogeneities rather than their permeability values.

In the second example (Case 2), the problem configurations are similar to that in Case 1, except that there are four materials (see labels in Fig. 6) with log permeability values of -13, -14, -12 and -9, respectively, where the background material has the highest log permeability. The true distribution of materials is shown in Fig. 6a. We start the simulation with an initial guess of three discs (Fig. 6b), which is quite different from the true field, and run up to 700 iterations. We fix the permeability of two higher permeable materials at $\log K_3 = -12$ and $\log K_4 = -9$, while assign the initial guesses $\log K_1 = -14$ and $\log K_2 = -15$, and allow them to be adjustable after 200 iterations. In this example, again we are interested in the spatial distribution of lower permeability materials embedded in the background material and the permeability of two lower permeable materials. The best permeability field out of 700 iterations is compared against the true field and the initial guess in Fig. 6c. The comparison shows that the inversion results characterize the 'true' zonation very well.

The RMSE and two lower permeabilities as functions of iterations for this case are illustrated in Fig. 7. An additional inverse model run with fixed permeability at their true values is conducted and the RMSE is also compared in the figure. Again, it appears that the RMSE is not sensitive to the initial guess of two lower permeability values. Because the reduction of RMSE for the case with fixed true permeability represents the evolution of the material distribution, two almost identical RMSEs suggest that the spatial distribution of the materials is much more important than the permeability values in fitting the observed hydraulic heads.

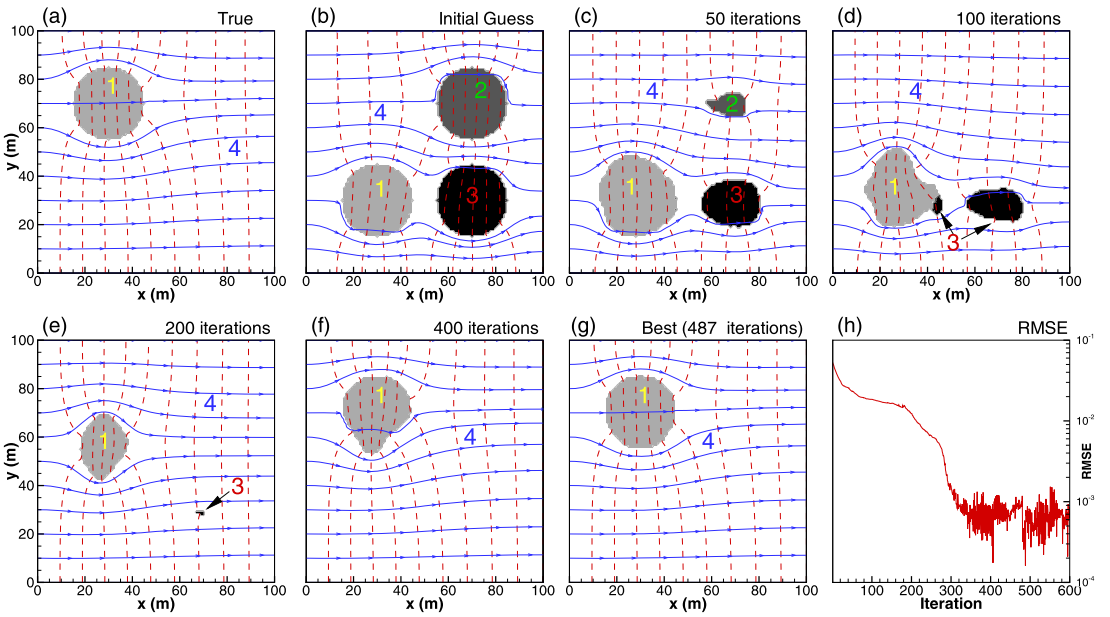

Fig. 8. Evolution of lower permeable inclusions for Case 3, where the true field has one lower permeable material (a), but the guess field has three lower permeable materials because of lacking accurate information about the number of materials. Plots (b)–(f) illustrate some snapshots of the evolution, plot (g) is the best fit out of 600 iterations, and plot (h) shows the RMSE.

6.2. Unknown number of materials

In the next two examples (Cases 3 and 4), we want to test the behavior of the algorithm when the number of materials is unknown. In both cases, the problem configurations and the locations of head measurements are the same as in Case 1. In Case 3, there are two materials: a lower permeable material of $\log K_1 = -12$ embedded in the background material of $\log K_4 = -9$ (Fig. 8a). Suppose that we do not know exactly the number of materials in the domain and guess that there may exist two additional materials with known permeability values $\log K_2 = -13$ and $\log K_3 = -14$. We start the guess material distribution as shown in Fig. 8b, where materials 2 and 3 do not exist in the true field and the location of material 1 is far away from its true location. As expected, the size of both materials 2 and 3 decreases (Fig. 8c) in the iterative process and they disappear at about 70 and 202 iterations, respectively (Fig. 8d, e). Only after disappearance of these no-existing materials does material 1 start to move upward and get close the true location (Fig. 8e, f). The best location and shape of material 1 is selected based on the smallest RMSE out of 600 iterations and is depicted in Fig. 8g, which is almost identical to the true one. The RMSE for this case is illustrated in Fig. 8h. It is seen from Fig. 8h that there exist two fast reduction segments in the RMSE curve (iterations 1–50, and 200–300). The first fast reduction corresponds to the shrinkage of material 2, and the second one to adjustment of the location for material 1. The RMSE is almost monotonically decreases in these two segments. After 300 iterations, the RMSE starts to oscillate, corresponding to adjusting the shape of material 1.

In Case 4, we consider a different scenario where there are three materials in the true permeability field: two lower permeable materials of $\log K_1 = -12$ and $\log K_2 = -14$ embedded in the background material with $\log K_3 = -9$, but we pretend that there is only one lower permeable material with $\log K_1 = -12$. The evolution of the material zonation is illustrated in Fig. 9, where plot (a) represents the true field, and plot (b) is our initial guess field, which is a large disc located at the center of the model domain because we do not have prior information about the true zonation. It is interesting to note that in early iterations the lower permeable zone starts to stretch along the direction in which two true lower permeable materials align, and it then breaks into two pieces at about iteration 80 (Fig. 9c). These two pieces then gradually move to the locations of the true lower permeable zones, although their sizes are small at this stage, comparing to the true ones (Fig. 9d). It is noted that the lower permeable zones will not grow when they are not at the right locations, because their growing at wrong locations will most likely increase the head residual. As soon as they reach the true locations, they start to grow (Fig. 9d, e, f). The best fit based on the smallest RMSE out of 800 iterations is shown in Fig. 9g, which is almost identical to the true field, except that now the permeability values for two lower permeable zones are the same because we assume that there is only one lower permeable material in the domain. The RMSE for all 800 iterations is depicted in Fig. 9h. This example also confirms our conclusion from Case 2 that the spatial distribution of the lower permeable materials is more important than their permeability values in fitting the observed heads. These two examples indicate that this level set algorithm is capable of identifying material zonation without accurate prior knowledge about the number of materials in the model domain.

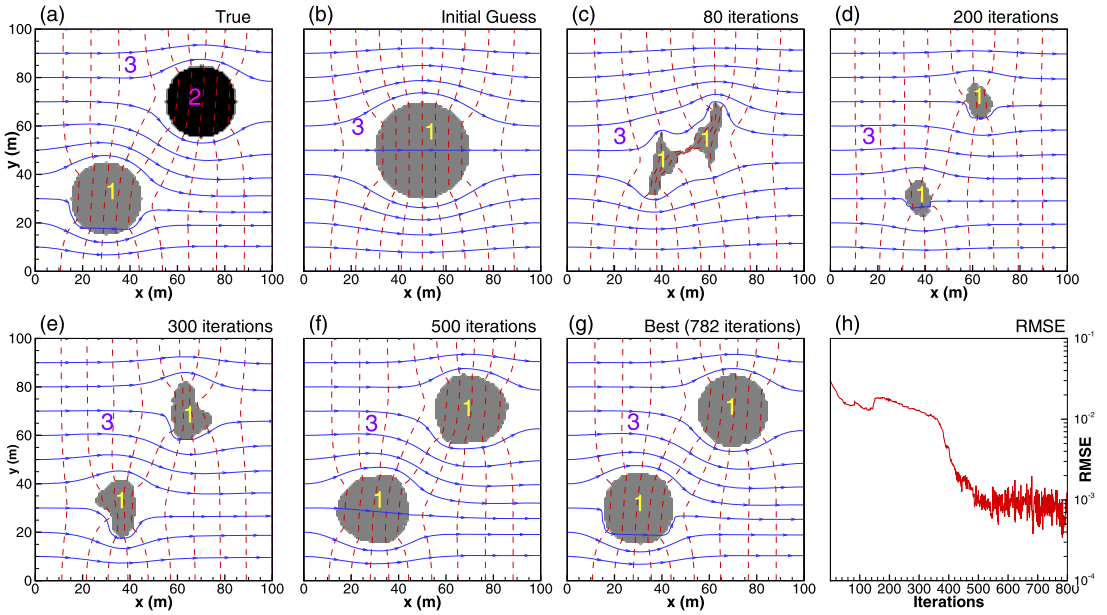

Fig. 9. Evolution of lower permeable inclusions for Case 4, where the true field has two lower permeable materials (a), but the guess field has one lower permeable material because of lacking accurate information about the number of materials. Plots (b)–(f) illustrate some snapshots of the evolution, plot (g) is the best fit out of 800 iterations, and plot (h) shows the RMSE.

6.3. Sensitivity of estimated zonation structure to initial guess field

In this subsection, we want to investigate the sensitivity of the estimated zonation on the initial guess field. The problem configurations, including the flow domain, boundary conditions and the true material zonation, are the same as those in Case 1, except that the number of measurements is increased to 361 (a 19×19 array). The reason for using the denser measurements is first to demonstrate that the discrepancy between the true and estimated zonation as shown in Figs. 4 and 6 is mainly due to lack of information, not to numerical problems.

The evolution of material zonation for five cases (named as Cases A–E) with different initial guess fields is depicted in Fig. 10, where the top row is for initial guesses, the middle row for snapshots at iteration 80, and the bottom row for the best result out of 600 iterations for each case.

Case A starts with the same initial guess field as that in Case 1. However, the best material zonation for Case A (Fig. 10-A3) is very close to the true one and has been significantly improved over the estimated zonation in Case 1, simply because of more head measurements included.

In Case B, two lower permeable materials are connected in the initial guess, but the algorithm is able to evolve each material such that the best estimated zonation is quite similar to the true one. The locations and the shapes of two lower permeable materials are the same in Cases C and D, but the different materials have been assigned. It is noted that, while the locations and the shapes of two lower permeable materials are correctly identified, in Case D, two materials have been switched. This is because, as discussed before, the locations and the shapes of lower permeable materials are more important than their actual permeability values. The flow field as indicated by head contour lines and streamlines for Case D (Fig. 10-D3) is very close to the true flow field, even though the permeability values for these lower permeable zones have been switched. In Case E, the locations of the initial lower permeable materials are the same as in Case A, but their sizes are much smaller. As the iterative process starts, material 2 quickly shrinks and disappears, and material 1 starts to grow and eventually becomes closer to the true material 1. The disappearance of the material 2 is mainly due to the combination of the small size and its larger permeability contrast with the background material. A fast reduction of the objective function may be easily achieved by simply eliminating the higher contrast materials rather than moving them. Even if material 2 in the guess field is placed at the true location, it may still disappear if its size is small, because locally the flow field in the earlier iterations may be significantly different from the true flow field. The lower permeable zone with a smaller permeability contrast will likely to survive, because its existence has a smaller impact on the flow field. This example implies that the size matters. It is our experience that, whenever possible, one should always start with large material zones in the guess field.

It is seen from this set of cases that qualitatively this level set method is not very sensitive to the initial guess field, and model runs starting with different initial guess fields may result to similar zonation structures, as long as the sizes of the material zones in the initial guess field are big enough. The algorithm is quite robust in identifying the material zonation.

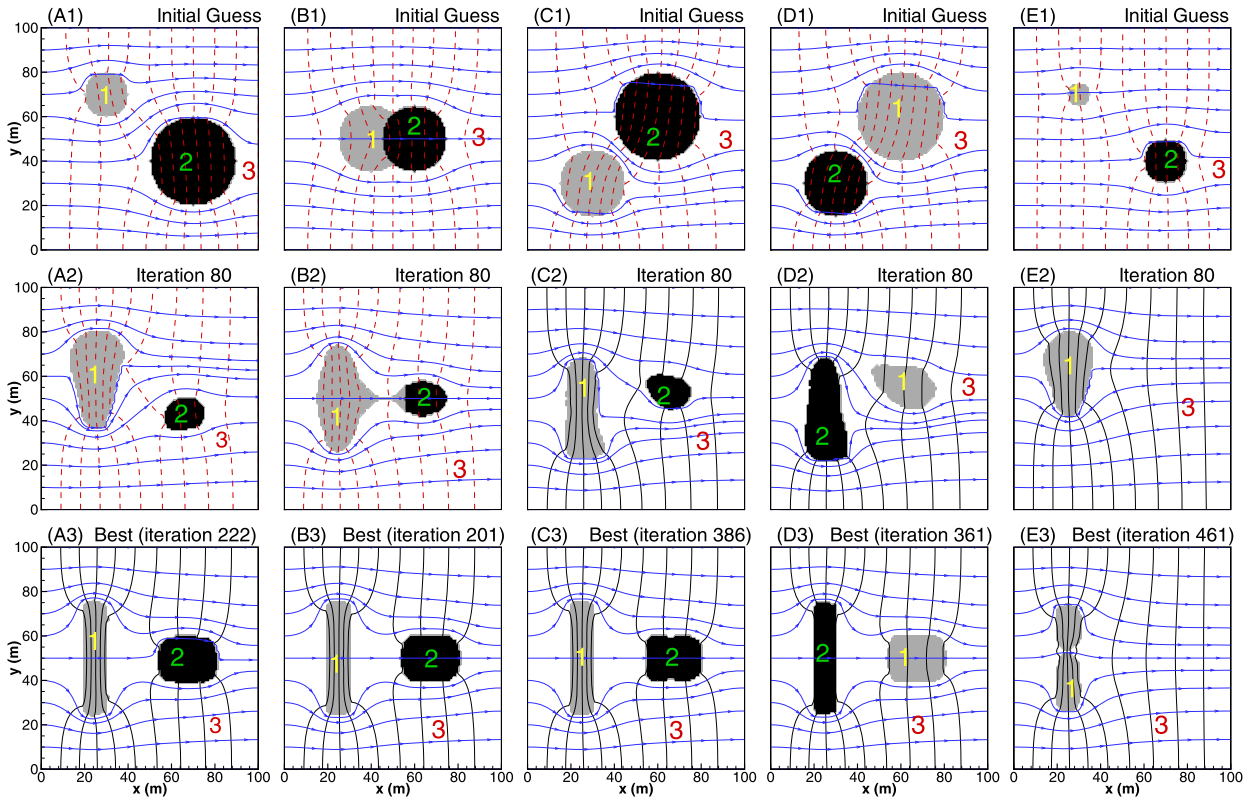

Fig. 10. Sensitivity of inverse results on the initial guess field. The true zonation is the same as that in Case 1. Top row shows 5 initial guesses, the middle row for their corresponding snapshots at iteration 80, and the bottom row for the best results.

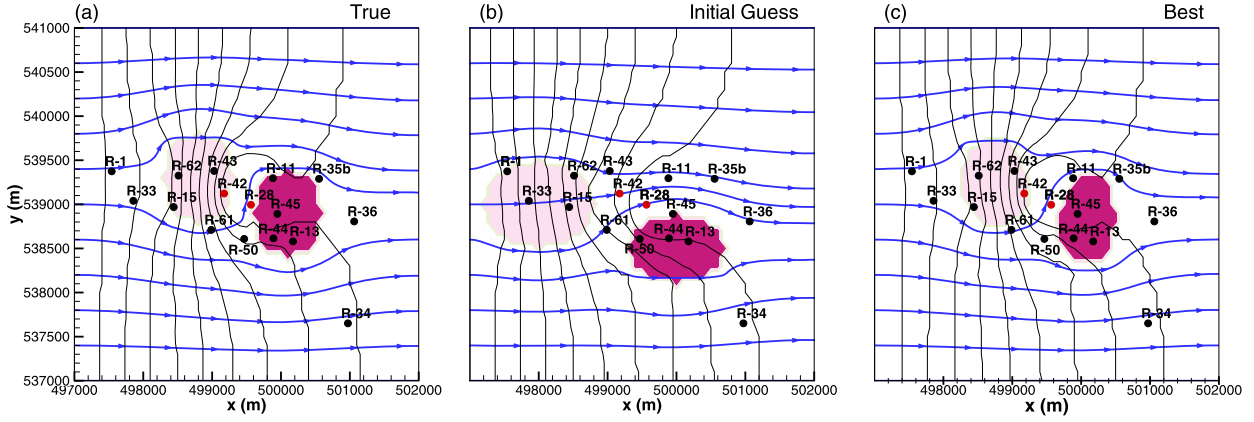

Fig. 11. Comparison of (a) the true, (b) initial guess, and (c) the best results in terms of the minimum residual from 100 iterations, which has three materials. The contours and streamlines represent the flow field at 200 days.

6.4. Application to LANL site

In the last example (Case 5), we consider a more realistic transient groundwater flow problem based on the Chromium contamination site in the regional aquifer at the Los Alamos National Laboratory [39,40]. Because the flow in the aquifer is nearly horizontal, we treat the groundwater flow as two-dimensional with a rectangular domain of $L_x = 5{,}000$ m and $L_y = 4{,}000$ m. The boundary conditions are given as: constant head at the western and the eastern boundaries as 1,001 m and 1,000 m, respectively, and no-flow on two lateral boundaries. Overall, the flow is along the x direction, under a hydraulic gradient of 0.0002. There are 14 site observation wells that are applied in this study (the well locations are shown in Fig. 11 as black dots). There are 22 transient drawdown data at each observation well, in response to pumping at wells R-28 and R-42 (red dots in Fig. 11) with variable pumping rates: 20 kg/s from $t = 0{\sim}200$ days at R-28, and 20 kg/s during

$t = 400\sim600$ days at R-42 (the synthetic pumping tests are designed to be consistent with actual field activities conducted at the site). The contours of hydraulic head and the streamlines in the figure represent the flow field at 200 days. It should be noted that both observation wells and pumping wells are concentrated in a small area of the domain, which makes it difficulty to infer the permeability field in the regions that are far away from the wells. While the flow domain and well placement are taken from the real site, the 'true' spatial distribution of the lower permeable zones are assumed for the purpose of testing the level set method.

Fig. 11a depicts the 'true' hydraulic conductivity field (in m/s) with two lower permeable zones $\log K_1 = -3.3$ and $\log K_2 = -4.9$ embedded in a background medium of $\log K_3 = -1.5$. The initial guess field and the best estimation (lowest RMSE) among 600 iterations are shown in Fig. 11b–c. Again, it is seen that the best estimation is quite similar to the 'true' field.

7. Conclusions and discussions

In this study, through mathematically rigorous derivations, we extended the level set method for identifying zonation in a binary system [1,2] to an arbitrary number of materials with unknown permeability (permeability is assumed to be uniform within each material), and obtained an expression for the propagation velocity of material interfaces and an expression for updating permeability for all materials. In each iteration, the propagation velocity at points on any material interface is proportional to the permeability contrast between materials on the two sides of the interface, the sensitivity of the head to permeability, and the residual between the simulated and the observed head. The update to permeability value of each material depends on the residual between the observed and the simulated hydraulic heads, weighted by the sensitivity of the head to permeability, integrated over each material zone. This update is consistent with the steepest descent direction of the objective function. The approach has been tested using a few examples that involve three or four materials with steady-state or transient head measurements in synthetic or real-world groundwater flow systems. The inversion results are quite reasonable. The approach is also capable of identifying the material zonation when the number of materials is not known exactly. Through these examples, it is demonstrated that, in inverse modeling, it is more important to identify the locations and the shapes of heterogeneities than their permeability values.

The proposed approach ensures that theoretically the residual is always decreasing during the iterative process, which is also a drawback of the approach, because the solution could be a local minimum. The evolution of the material zonation, solved from the initial value problem of the LSFs, is of course dependent on the initial LSFs or equivalently on the initial guess field. Numerical investigation on the sensitivity of the inversion results to the initial guess field indicates that the results are not very sensitive to the initial guess. In other words, model runs starting with different initial guess fields may evolve to the similar final zonation structures. Our experience is that the sizes of the material zones in the initial field should not be too small, or otherwise they may quickly disappear, especially for those materials that have large permeability contrasts with the background material. The effect of the initial field can be further reduced by, for example, using some prior information (such as well log data or outcrops) to condition the zonation structure at the measurement locations of the permeability field. The conditioning may be achieved by selecting the initial guess to satisfy the direct measurements and then enforcing the zero propagation velocity around these condition points during the iterative process. One may also initiate a set of inverse model runs, each of which starts with random locations of the initial guess and random initial permeability, and the best solution (smallest RMSE) among these inverse runs may be considered as the solution to the inverse problem.

Although in theory the method may work for any arbitrary number of materials, in practice, it may not work for an extremely large number of materials because this method relies on the permeability contrast to drive the interface propagation. The performance of this method will deteriorate if permeability contrasts are small. However, if the permeability values of two or more stratigraphic units are close, it is typical in hydrologic inverse modeling to combine them into one material in the model.

References

[1] F. Santosa, A level-set approach for inverse problems involving obstacles, ESAIM Control Optim. Calc. Var. 1 (1996) 17–33.
[2] Z. Lu, B.A. Robinson, Parameter identification using the level set method, Geophys. Res. Lett. 33 (6) (2006) 1–4.
[3] W.W.-G. Yeh, Review of parameter identification procedures in groundwater hydrology: the inverse problem, Water Resour. Res. 22 (2) (1986) 95–108.
[4] D. McLaughlin, L.R. Townley, A reassessment of the groundwater inverse problem, Water Resour. Res. 32 (5) (1996) 1131–1161.
[5] S. Finsterle, Multiphase inverse modeling, Vadose Zone J. 3 (3) (2004) 747–762.
[6] Y. Emsellem, G. De Marsily, An automatic solution for the inverse problem, Water Resour. Res. 7 (5) (1971) 1264–1283.
[7] J. Carrera, S.P. Neuman, Estimation of aquifer parameters under transient and steady state conditions: 3. Application to synthetic and field data, Water Resour. Res. 22 (2) (1986) 228–242.
[8] A. Keidser, D. Rosbjerg, A comparison of four inverse approaches to groundwater flow and transport parameter identification, Water Resour. Res. 27 (9) (1991) 2219–2232.
[9] N.-Z. Sun, W.W.-G. Yeh, Identification of parameter structure in groundwater inverse problem, Water Resour. Res. 21 (6) (1985) 869–883.
[10] M.T. Ayvaz, Simultaneous determination of aquifer parameters and zone structures with fuzzy c-means clustering and meta-heuristic harmony search algorithm, Adv. Water Resour. 30 (11) (2007) 2326–2338.
[11] M.J. Eppstein, D.E. Dougherty, Simultaneous estimation of transmissivity values and zonation, Water Resour. Res. 32 (11) (1996) 3321–3336.
[12] F.T.-C. Tsai, N.-Z. Sun, W.W.-G. Yeh, Global–local optimization for parameter structure identification in three-dimensional groundwater modeling, Water Resour. Res. 39 (2) (2003) 1–14.

[13] F.T.-C. Tsai, N.-Z. Sun, W.W.-G. Yeh, Geophysical parameterization and parameter structure identification using natural neighbors in groundwater inverse problems, J. Hydrol. 308 (1) (2005) 269–283.
[14] F.T.-C. Tsai, W.W.-G. Yeh, Characterization and identification of aquifer heterogeneity with generalized parameterization and bayesian estimation, Water Resour. Res. 40 (10) (2004) 1–12.
[15] C.-P. Tung, C.-C. Tang, Y.-P. Lin, Improving groundwater-flow modeling using optimal zoning methods, Environ. Geol. 44 (6) (2003) 627–638.
[16] Y.-C. Chiu, Application of differential evolutionary optimization methodology for parameter structure identification in groundwater modeling, Hydrogeol. J. 22 (8) (2014) 1731–1748.
[17] S. Osher, J.A. Sethian, Fronts propagating with curvature-dependent speed: algorithms based on Hamilton–Jacobi formulations, J. Comput. Phys. 79 (1) (1988) 12–49.
[18] M. Burger, A framework for the construction of level set methods for shape optimization and reconstruction, Interfaces Free Bound. 5 (3) (2003) 301–330.
[19] J. Lie, M. Lysaker, X.-C. Tai, A piecewise constant level set framework, Int. J. Numer. Anal. Model. 2 (4) (2005) 422–438.
[20] M. Lien, I. Berre, T. Mannseth, Combined adaptive multiscale and level-set parameter estimation, Multiscale Model. Simul. 4 (4) (2005) 1349–1372.
[21] O. Dorn, R. Villegas, History matching of petroleum reservoirs using a level set technique, Inverse Probl. 24 (3) (2008) 035015.
[22] M. Cardiff, P. Kitanidis, Bayesian inversion for facies detection: an extensible level set framework, Water Resour. Res. 45 (10) (2009) 1–15.
[23] M. Kilmer, E. Miller, M. Enriquez, D. Boas, Cortical constraint method for diffuse optical brain imaging, in: Optical Science and Technology, the SPIE 49th Annual Meeting, International Society for Optics and Photonics, 2004, pp. 381–391.
[24] S. Wang, M.Y. Wang, Radial basis functions and level set method for structural topology optimization, Int. J. Numer. Methods Eng. 65 (12) (2006) 2060–2090.
[25] I. Berre, M. Lien, T. Mannseth, A level-set corrector to an adaptive multiscale permeability prediction, Comput. Geosci. 11 (1) (2007) 27–42.
[26] G. Pingen, M. Waidmann, A. Evgrafov, K. Maute, A parametric level-set approach for topology optimization of flow domains, Struct. Multidiscip. Optim. 41 (1) (2010) 117–131.
[27] A. Aghasi, M. Kilmer, E.L. Miller, Parametric level set methods for inverse problems, SIAM J. Imaging Sci. 4 (2) (2011) 618–650.
[28] H. Chang, D. Zhang, Z. Lu, History matching of facies distribution with the EnKF and level set parameterization, J. Comput. Phys. 229 (20) (2010) 8011–8030.
[29] O. Bernard, D. Friboulet, P. Thévenaz, M. Unser, Variational b-spline level-set: a linear filtering approach for fast deformable model evolution, IEEE Trans. Image Process. 18 (6) (2009) 1179–1191.
[30] D. Zhang, Z. Lu, An efficient, high-order perturbation approach for flow in random porous media via Karhunen–Loeve and polynomial expansions, J. Comput. Phys. 194 (2) (2004) 773–794.
[31] R.L. Graham, D.E. Knuth, O. Patashnik, Concrete Mathematics: A Foundation for Computer Science, Addison & Wesley, 1994.
[32] I.M. Gelfand, R.A. Silverman, et al., Calculus of Variations, Courier Corporation, 2000.
[33] T. Padmanabhan, Quantum Field Theory: The Why, What and How, Springer, 2016.
[34] J. Sykes, J. Wilson, R. Andrews, Sensitivity analysis for steady state groundwater flow using adjoint operators, Water Resour. Res. 21 (3) (1985) 359–371.
[35] J. Zhu, T.-C. J. Yeh, Characterization of aquifer heterogeneity using transient hydraulic tomography, Water Resour. Res. 41 (7) (2005).
[36] Z. Lu, V.V. Vesselinov, Analytical sensitivity analysis of transient groundwater flow in a bounded model domain using the adjoint method, Water Resour. Res. 51 (7) (2015) 5060–5080.
[37] M. Sussman, P. Smereka, S. Osher, A level set approach for computing solutions to incompressible two-phase flow, J. of Comput. Phys. 114 (1) (1994) 146–159.
[38] G.A. Zyvoloski, B.A. Robinson, Z.V. Dash, L.L. Trease, Summary of the models and methods for the FEHM application–a Finite-Element Heat- and Mass-Transfer code, LA-13307-MS, 1997.
[39] V.V. Vesselinov, D. O'Malley, D. Katzman, Model-assisted decision analyses related to a chromium plume at Los Alamos National Laboratory, in: WM-SYM2015, Phoenix, Arizona, USA, 2015.
[40] V.V. Vesselinov, D. O'Malley, D. Katzman, ZEM: integrated framework for real-time data and model analyses for robust environmental management decision making, in: WMSYM 2016, Phoenix, Arizona, USA, 2016.